

X-ray Scattering and Magnetic Susceptibility Study of doped CuGeO_3

Y. J. Wang

*Center for Materials Science and Engineering and Department of Physics,
Massachusetts Institute of Technology, Cambridge, MA 02139*

Y. J. Kim

Physics Department, Brookhaven National Laboratory, Upton, NY 11973

R. J. Christianson, S. C. LaMarra, and F. C. Chou

Center for Materials Science and Engineering, Massachusetts Institute of Technology, Cambridge, MA 02139

T. Masuda, I. Tsukada, and K. Uchinokura

*Department of Applied Physics, The University of Tokyo,
7-3-1 Hongo, Bunkyo-ku, Tokyo 113-8656, Japan*

R. J. Birgeneau

*Department of Physics, University of Toronto, Toronto, Ontario M5S 1A7, Canada
(Dated: November 21, 2018)*

We report comprehensive synchrotron x-ray scattering and magnetic susceptibility studies of the doped spin-Peierls materials $\text{Cu}_{1-x}\text{Zn}_x\text{GeO}_3$ and $\text{CuGe}_{1-y}\text{Si}_y\text{O}_3$. Temperature versus dopant concentration phase diagrams are mapped out for both Zn and Si dopants. The phase diagrams of both $\text{Cu}_{1-x}\text{Zn}_x\text{GeO}_3$ and $\text{CuGe}_{1-y}\text{Si}_y\text{O}_3$ closely resemble that of $\text{Cu}_{1-x}\text{Mg}_x\text{GeO}_3$, including the observation that the spin gap is established at a much higher temperature than the temperature at which the spin-Peierls dimerization attains long-range order. The spin-Peierls transitions in doped samples exhibit unusual phase transition behavior, characterized by highly rounded phase transitions, Lorentzian squared lineshapes, and very long relaxation times. Phenomenological explanations for these observations are given by considering the effects of competing random bond interactions as well as random fields generated by the dopants. We have also confirmed the reentrance of the spin-Peierls phase when the temperature is lowered through the antiferromagnetic ordering transition. The low temperature re-entrance of the spin-Peierls phase has been explained speculatively using a local phase separation scheme between the spin-Peierls phase and the Néel phase.

PACS numbers: 75.30.Kz, 75.10.Jm, 75.40.Cx, 75.80.+q

I. INTRODUCTION

Low-dimensional quantum spin systems exhibit a variety of intriguing and often counter-intuitive properties. A prominent example of such a material is the spin-Peierls (SP) system, which consists of an array of one-dimensional (1D) antiferromagnetic spin-chains with $S=\frac{1}{2}$ on a deformable three-dimensional (3D) lattice. Below the spin-Peierls transition temperature, T_{SP} , the spin-chains dimerize and a gap opens in the magnetic excitation spectrum. The discovery of an inorganic SP compound CuGeO_3 made possible a systematic study of impurity effects on SP systems.¹ Despite extensive experimental and theoretical efforts devoted to the study of the effects of doping on the magnetic and structural phase transitions in CuGeO_3 , controversies still remain on several fronts. One major unresolved issue is the temperature versus concentration phase diagram for both within-chain and between-chain dopants.^{2,3,4,5,6,7,8,9,10,11,12} The phase diagram has shown certain unusual characteristics as revealed by different techniques: on the one hand, the phase behavior is so complex that there are continuing debates about the physics underlying nearly every sin-

gle part of the phase diagram. On the other hand, there exists surprising similarities in the phase behavior for different dopants, irrespective of the type and atomic size of the dopant ions, the magnetic moment size, or the doping geometry. In some theoretical models, there exists a close relation between the spin-Peierls transition and the subsequent antiferromagnetic phase transition which occurs at a lower temperature in samples with a dopant concentration x below a critical value x_c . Our own results suggest that the suppression of the spin-Peierls phase as a result of doping has no causative correlation with the emergence of the low-temperature antiferromagnetic phase except for the fact that the dopants create unpaired Cu spins. The lack of direct correlation is manifested most clearly in a comparative study of magnetic and non-magnetic ion dopings where the high temperature suppression of the SP phase seems to follow a quite universal behavior with different dopants while the low temperature occurrence of the antiferromagnetic phase reflects the different magnetic properties of the individual magnetic ion dopants.

Currently, for within-chain doping studies, both magnetic and non-magnetic ions have been utilized, including Zn, Mg and Ni.^{2,3,4,5,8,9,10,11,12,13,14,15,16,17} In early

work on doped CuGeO_3 , Zn was by far the most studied dopant. A rich amount of information has been accumulated with a variety of experimental techniques; however, it has turned out that $\text{Cu}_{1-x}\text{Zn}_x\text{GeO}_3$ is far from being the ideal system, because of concentration gradient effects and difficulties in fixing the exact Zn concentration.¹⁰ Despite these complications, we have continued x-ray scattering studies of Zn-doped samples in the hope that by directly comparing our experimental results with all extant ones, we can elucidate the underlying physics. $\text{CuGe}_{1-y}\text{Si}_y\text{O}_3$, on the other hand, currently serves as the sole system for studying between-chain doping effects.^{7,14,16} Accordingly, we have carried out x-ray scattering experiments on $\text{CuGe}_{1-y}\text{Si}_y\text{O}_3$ in parallel with our Zn studies. Finally, Mg doping, regarded as the ideal dopant for within-chain dopants, has been studied extensively by us and our results have been published in several previous papers.^{10,11,12,18} In this paper, we will focus on a comprehensive interpretation of the general phenomenology for both within-chain and between-chain dopings. We also will present in detail a phenomenological model for the overall phase behavior.

Studies of the effects of dopants on the spin-Peierls transition in CuGeO_3 started with the magnetic susceptibility measurements by Hase *et al.* right after the discovery of CuGeO_3 as the first inorganic spin-Peierls material.^{13,19} In that work, Hase *et al.* reported a systematic study of the dopant concentration versus temperature phase diagram using Zn as the dopant. Later, despite extensive experimental and theoretical efforts devoted to trying to confirm this phase diagram, more and more controversies seemed to turn up.^{3,13,14,15,16,19,20,21} Scattering experiments, arguably the most direct experimental technique for studying structural phase transitions, have provided invaluable insights into the phenomenology of doped CuGeO_3 . Neutron scattering experiments have been carried out by different groups.^{4,5,9,19} In particular, Martin *et al.*⁵ performed the first comprehensive neutron-scattering study of $\text{Cu}_{1-x}\text{Zn}_x\text{GeO}_3$. They discovered a temperature-concentration phase diagram in which the spin-Peierls phase transition temperature (T_{SP}) first decreased linearly with Zn concentration and then appeared to show a plateau-like behavior above about 2% Zn doping. The plateau was presumed to persist up to more than 5% Zn doping. Nevertheless, significant broadening of the SP superlattice diffraction peaks was observed in a 3.2% Zn-doped sample which suggests that the high doping spin-Peierls phase may not be a true independent phase. This phase diagram was clearly in contradiction with the one obtained by Hase *et al.* through susceptibility measurements.¹³ In the original phase diagram obtained by Hase *et al.*, there is a linear decrease of T_{SP} upon doping up to 2% Zn, which is in agreement with Martin *et al.*'s results. However, Hase *et al.* reported the disappearance of the SP transition above 2% Zn doping; this was indicated by the disappearance of the characteristic dip in the magnetic susceptibility curve, which reflects

the opening of the SP spin gap and therefore ordinarily signifies the onset of the SP transition.

At first glance, the above two phase diagrams seem to be irreconcilable with each other. However, if one takes a closer look at the experimental specifics, one finds that the discrepancy originates in part from the different approaches of two experimental techniques. Susceptibility measurements, as a macroscopic experimental technique, are primarily sensitive to long range order and less so to local fluctuations. Neutron scattering, on the other hand, given sufficiently coarse resolution and long scan times, can easily reveal the existence of short range fluctuations. The neutron scattering results reported by Martin *et al.* strongly suggest that the high doping SP phase is of short range order and hence not easily detected by magnetic susceptibility measurements. Thus, care must be taken in determining the phase diagram of the high doping phase. Similar ambiguities have been discovered in studies of Si-doped samples.

Thus, a systematic and detailed study using both susceptibility and scattering techniques should help to resolve some of the extant discrepancies. In this paper, we report a detailed synchrotron x-ray scattering and magnetic susceptibility study of the spin-Peierls transition in both $\text{Cu}_{1-x}\text{Zn}_x\text{GeO}_3$ and $\text{CuGe}_{1-y}\text{Si}_y\text{O}_3$. The paper is organized as follows: First we present the results for $\text{Cu}_{1-x}\text{Zn}_x\text{GeO}_3$ as a prototypical example to elaborate on the major experimental results. The general conclusions are applied to our study of $\text{CuGe}_{1-y}\text{Si}_y\text{O}_3$. We then present a phenomenological interpretation of our combined results, in which the important roles played by competing interactions, random fields and phase inhomogeneity will be emphasized.²²

In the next section, we describe the sample preparation and the experimental techniques used in this study. In Sec. III, our experimental results from x-ray scattering and magnetic susceptibility measurements are presented, including the experimentally determined phase diagrams for both Zn- and Si-doped CuGeO_3 . Finally, we will discuss various theoretical and experimental issues in Sec. IV.

II. EXPERIMENTAL DETAILS

A. Crystal Growth

The single crystals used in the experiment come from two sources. The $\text{CuGe}_{1-y}\text{Si}_y\text{O}_3$ single crystals were grown at the University of Tokyo using the traveling solvent floating zone method and preliminary sample characterization and magnetic susceptibility results have been published elsewhere.²³ The impurity concentration of these samples has been determined by inductively coupled plasma atomic emission spectroscopy (ICP-AES), with an accuracy of about 0.1%. The $\text{Cu}_{1-x}\text{Zn}_x\text{GeO}_3$ crystals were grown by the same method at MIT. Samples have a typical mosaic spread of less than 0.05° full-

TABLE I: Characterization of $\text{Cu}_{1-x}\text{Zn}_x\text{GeO}_3$ crystals. T_{SP} and T_N are determined from the magnetic susceptibility measurements (see Fig. 1).

x (nominal)	x (EPMA)	T_{SP} (K)	T_N (K)
0.0	< 0.003	14.10(5)	-
0.005	0.007(1)	13.5(1)	-
0.01	0.011(1)	12.6(1)	-
0.02	0.020(1)	10.5(1)	2.2
0.03	0.0235(10)	9.7(2)	2.75
0.043	0.0255(10)	9.2(3)	2.9
0.03	0.0270(15)	8.8(5)	3.1/3.8
0.046	0.034(3)	-	4.3
0.05	0.038(2)	-	4.4
0.06	0.038(5)	-	4.4

width at half-maximum at major Bragg diffraction peaks. The typical sample size used for both x-ray scattering and magnetic susceptibility measurements was about $3 \times 3 \times 1 \text{ mm}^3$. We prepared our samples by cutting them from the end of regular growths which have lengths over 5 cm. This procedure effectively eliminated the gradient induced in crystal growth caused by the different doping levels of the seed crystals.

In order to differentiate the intrinsic physics from extraneous effects caused by simple concentration gradients, a detailed and careful characterization of the samples is crucial. The electron probe microscope analysis (EPMA) method was used to determine the Zn doping concentrations. Twenty evenly spaced spots covering the whole sample surface were used in the EPMA measurements. The variations of concentrations were recorded as the uncertainties in the sample concentration. The sample characterization results are summarized in Table I. As shown in Table I, the actual Zn contents are always lower than the nominal ones in the high doping range, which is consistent with previously reported results.^{3,5} However, despite the great disparities between these two concentrations, the concentration gradients and fluctuations found over the surfaces remain relatively small and comparable to those in the Mg-doped samples.¹⁰ Moreover, the concentration variations have similar magnitudes for all samples, which suggests comparable effects, if any, on the observed SP phase transitions.

B. Synchrotron x-ray scattering

High resolution synchrotron x-ray scattering is a powerful tool in studying structural phase transitions. High-flux synchrotron x-ray radiation enables us to study both the critical fluctuations and the long range order. Our experiments were carried out at MIT-IBM beamline X20A at the National Synchrotron Light Source. The 8.5 keV x-ray beam was focused by a mirror, monochromatized by a pair of Ge (111) crystals, scattered from the sample, and analyzed by a Si (111) analyzer. Carefully cleaved samples were placed inside a Be can filled with helium

heat-exchange gas and mounted on the cold finger of a closed-cycle refrigerator. The measurements were carried out in each sample at the (1.5, 1, 1.5) SP dimerization peak position with the (H K H) zone in the scattering plane. The high momentum resolution of the synchrotron x-ray beam enabled us to measure intrinsic correlation lengths as large as 5000 Å; any system with a correlation length larger than this was considered to possess long-range order (LRO).

C. Magnetic susceptibility

The magnetic susceptibility of the identical samples used in the x-ray experiments has been measured using a commercial SQUID magnetometer (Quantum Design MPMS). The samples were mounted with the c axis parallel to the applied magnetic field, and the data were taken in a magnetic field of 500 Oe.

III. EXPERIMENTAL RESULTS

A. Magnetic susceptibility – Zn doping

Figure 1 shows the magnetic susceptibility as a function of temperature for all of the $\text{Cu}_{1-x}\text{Zn}_x\text{GeO}_3$ samples. The overall features are similar to previously reported results,^{7,8,10,12} showing a rapid suppression of the SP phase transition temperature upon doping and the appearance of a low temperature antiferromagnetic (AF) phase. For doped samples, the kink anomaly, which is a characteristic of the SP transition, is rounded. We determine T_{SP} in the susceptibility measurements from the maximum of the derivative of the kink anomaly and the Néel temperature, T_N , simply from the low-temperature cusp temperature. For samples with $x=0.0235$, 0.0255, 0.34, and 0.38, a sharp low-temperature cusp which signifies the onset of the AF state is observed. On the other hand, the susceptibility curve of the $x=0.027$ sample shows a broad low temperature peak with two cusp positions possibly corresponding to two Néel temperatures.

This is reminiscent of similar results obtained for Mg-doped samples by Masuda and coworkers.¹² Those authors carried out susceptibility measurements on a series of $\text{Cu}_{1-x}\text{Mg}_x\text{GeO}_3$ samples, and found a double peak feature in the low temperature susceptibility data, for x in the neighborhood of 0.023. In their study, it was argued that there exists a first order phase transition as a function of x , between a dimerized antiferromagnetic phase and a uniform antiferromagnetic phase, so that around the critical concentration $x_c \simeq 0.023$, two AF transitions appear because of the microscopic phase separation between these two phases. Detailed comparison of the magnetic susceptibilities of Zn- and Mg- doped samples yield many similarities, as expected. In Ref. 12, the sample with the highest Mg-doping without the

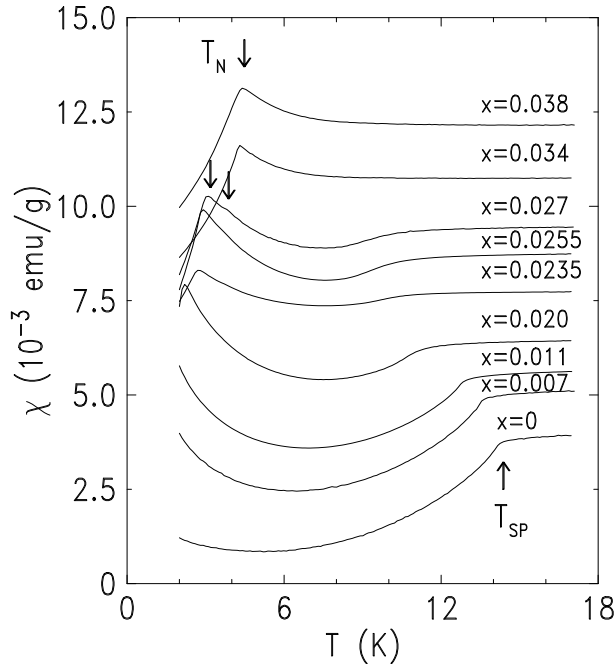


FIG. 1: The magnetic susceptibility as a function of temperature for various Zn-doped samples. Each curve is shifted by 10^{-3} emu/g for clarity.

broadening feature had a Néel transition around 2.9 K and $x_{Mg} = 0.0229$. The low threshold started with $x_{Mg} = 0.0237$ in which there existed a broadened cusp spanning from 3.2 K to 3.9 K. The cusp peaked more to the low temperature side with the weight gradually shifting to the high temperature side as the concentration was increased.¹² We note in Fig. 1 similar behavior in our Zn-doped samples, with the $x = 0.0255$ Zn-doped sample showing a single cusp at 2.9K, while the $x = 0.027$ sample shows a broadened cusp over the temperature range from 3.1 K to 3.8 K. For $x=0.027$, the left side of the cusp is much higher than the right side suggesting that this sample is closer to the lower temperature threshold of the peak broadening phenomenon. Unfortunately, we do not have a range of doping concentrations from $x=0.027$ to $x=0.034$ which could give us a more complete view of the gradual shift of the weights. The important point is, however, that we have confirmed that the regime where the susceptibility shows significant broadening coincides with the region where, as we shall discuss in the next subsection, the SP phase begins to lose LRO while substantial superlattice scattering intensity is nevertheless still observable.¹¹ Therefore, the Néel transition broadening must somehow be correlated with the loss of LRO of the SP phase.

B. X-ray scattering – Zn doping

The instrumental resolution function was experimentally measured at the (3, 0, 0) Bragg peak, which has

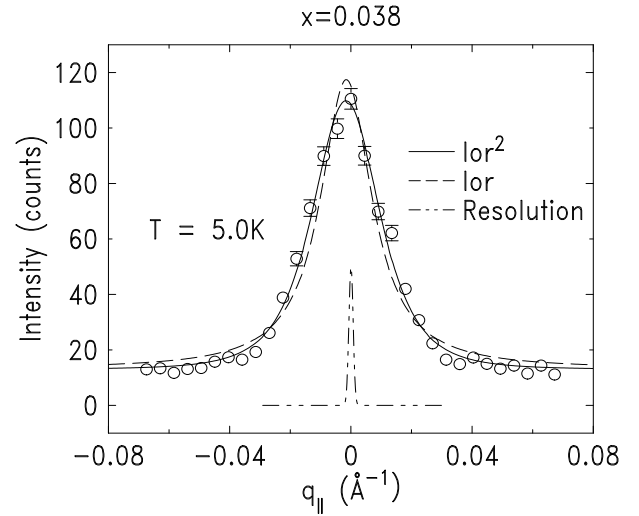


FIG. 2: Longitudinal scan profile of the superlattice peak, (1.5, 1, 1.5), at $T=5$ K for $x=0.038$. The solid and dashed line shows the corresponding results fitted by Lorentzian and Lorentzian squared lineshapes convoluted with the instrumental resolution function.

a Q value close to that of the (1.5, 1, 1.5) dimerization peak. The determination of the intrinsic line-shape is complicated by the existence of the two-length scale phenomenon as has been discussed in previous work by some of us.²⁴ Since two superimposed profiles corresponding to two length scales were always present in the critical scattering in the close vicinity of the SP transition for $x \leq 0.02$ samples, a unique determination of the intrinsic cross-section was difficult. However, only a single scattering profile was observable in the critical scattering for $x \geq 0.02$ samples, where dopant effects play a more important role than the near surface dislocation effects which are presumably responsible for the large length scale fluctuations in samples with LRO. For typical second order phase transitions, the critical scattering cross section assumes a Lorentzian lineshape. Any deviation from this line-shape can provide information on the effects of disorder on the underlying phase transition.

In Fig. 2, we show the low temperature (1.5, 1, 1.5) superlattice peak profile for the $x=0.038$ sample. It is evident that the resolution function is much narrower than the intrinsic cross section. Both Lorentzian and Lorentzian squared cross sections have been used to fit the data. The Lorentzian squared lineshape gives a discernably better fit than a simple Lorentzian lineshape.

Figure 3(a) shows the temperature dependence of the (1.5, 1, 1.5) dimerization peak intensity for various $\text{Cu}_{1-x}\text{Zn}_x\text{GeO}_3$ samples. We normalize the intensity of each sample data set using the dimerization peak intensity at 5 K. As is obvious in the figure, in sharp contrast to the transition in pure CuGeO_3 , the SP transitions for the doped samples are noticeably rounded, and further the rounding increases progressively with increasing dopant concentration. We believe that this substan-

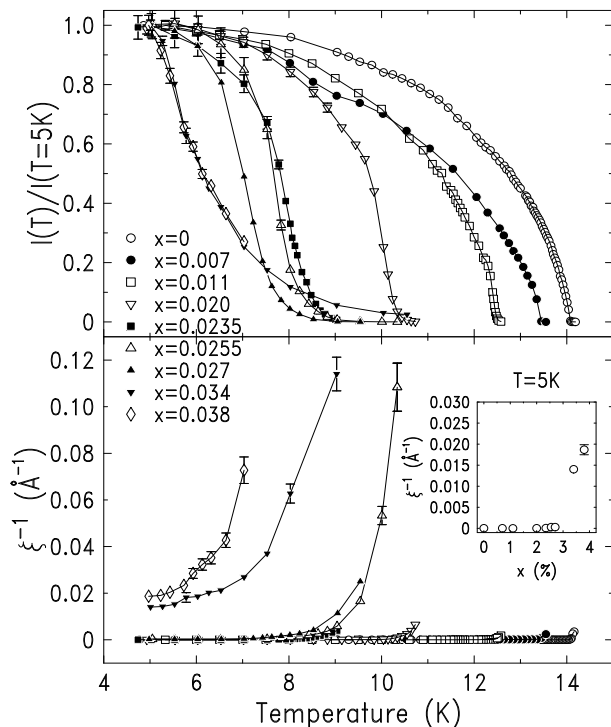


FIG. 3: The (1.5, 1, 1.5) SP peak intensity (a) and the corresponding inverse correlation length (b) as functions of temperature for various Zn-doping concentrations. The inset shows the impurity-concentration dependence of the low-temperature SP inverse correlation length

tial rounding is intrinsic and cannot simply be accounted for by local concentration gradients for the following reasons: (i) The impurity concentration is too low to create any substantial correlated effect.²⁵ (ii) There exists a monotonic increase of the rounding in the order parameter as the doping concentration is increased, while experimentally the measured concentration gradients are of similar magnitude for all of the samples studied. For example, the $x=0.038$ sample has a concentration variance of less than 0.2%, from Table I. However, that sample's SP dimerization peak intensity increases sufficiently gradually as the temperature is lowered that it does not achieve saturation for the whole temperature range studied. In sharp contrast, no significant rounding was found in the $x=0.011$ sample which has a similar concentration variance.

Not only does the order parameter temperature dependence change dramatically upon doping, the corresponding saturation correlation length also behaves quite differently from that in the undoped sample. Figure 3(b) shows the temperature dependence of the longitudinal inverse correlation length for the different $\text{Cu}_{1-x}\text{Zn}_x\text{GeO}_3$ samples. The minimum inverse correlation length which the sample achieves as a function of x is plotted in the inset. Unlike the pure material, in which very near T_{SP} the inverse correlation length decreases linearly to zero as T_{SP} is approached from above because of the second

length scale critical fluctuations, the inverse correlation length of the doped samples appears to approach zero in an asymptotic way without a clear signature of the exact temperature at which it becomes zero. This complication makes an unequivocal determination of T_{SP} difficult. Within our experimental accuracy, samples attain LRO (that is, the correlation length exceeds 5000 Å) only for $x \leq 0.027$. Substantial intensity is still observable at the superlattice peak positions for the $x=0.034$ and $x=0.038$ samples which have $x > x_c \equiv 0.027$, although the superlattice peaks are not resolution-limited in width. The critical dopant concentration, x_c , which we have determined for $\text{Cu}_{1-x}\text{Zn}_x\text{GeO}_3$ is slightly higher than that for the $\text{Cu}_{1-x}\text{Mg}_x\text{GeO}_3$ samples. However, this could be due in part to the different techniques used in determining the concentrations.

In Fig. 4, we show the results from the fits for the peak intensity, which for LRO is the order parameter squared, and the inverse correlation length, ξ^{-1} for samples with $x=0.011$ and $x=0.0235$. Also plotted is the diffuse scattering intensity at the wing ($\delta q = 0.022$ Å⁻¹) of the dimerization superlattice peak, which is a measure of the amplitude of the critical fluctuations. The transition is slightly broadened as compared to the SP transition in pure CuGeO_3 . This is reflected both in the smearing of the order parameter onset temperature and the temperature range of the diffuse scattering. The inverse correlation length follows more or less a linear relationship with temperature. For the samples with $x=0.0235$, the broadening in the temperature dependence of both the order parameter and the diffuse scattering has increased significantly. The corresponding inverse correlation length first exhibits a linear relationship as a function of temperature with decreasing temperature. However, close to the transition, $T \leq 9.5$ K, the rate of the divergence slows down and ξ^{-1} appears to approach zero asymptotically, that is, with zero slope. It is interesting to note that if the linear behavior is extrapolated to intersect the temperature axis, one obtains a temperature which roughly matches that of the maximum of the diffuse scattering.

SP transitions in doped samples have shown unconventional characteristics that are absent in typical second-order phase transitions. One of these is that when the doped system undergoes a SP transition, the times for the system to reach phase equilibrium are anomalously long. In x-ray scattering experiments, this is reflected in a continuous change in the peak intensity and width as a function of time. This anomaly manifests itself in pronounced thermal hysteresis in the order parameter measurements if the system is not kept sufficiently long at each temperature. This slow dynamics behavior is not observed in pure CuGeO_3 . Under the same experimental conditions, upon rapid change of temperature by several degrees, the pure system achieves equilibrium within minutes, in sharp contrast to the highly doped samples. We characterized the slow dynamics by monitoring the intensity of the superlattice peak after a sudden change in temperature as a function of time while keeping the

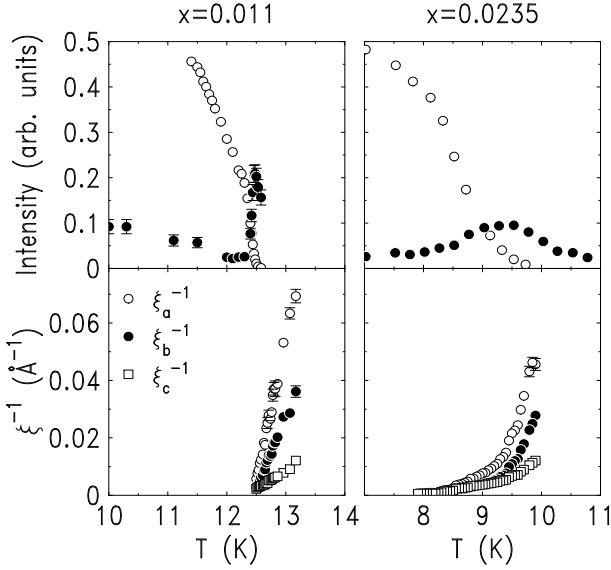


FIG. 4: Top: Peak intensity of the superlattice peak (empty symbols) and the diffuse scattering intensity at $(1.5\ 1.03\ 1.5)$, plotted as a function of temperature. Bottom: Inverse correlation length of the critical scattering along the a , b , and c directions.

final temperature constant. The time scans for the system in equilibrium show an oscillating behavior with the centerline remaining flat. The oscillations reflect the temperature fluctuations at the sample place and agree well with the temperature fluctuation patterns recorded from the temperature controller.

Figure 5 shows representative time scans for $x=0.0235$ for both heating and cooling temperature runs on a semi-logarithmic scale. After the sample was quenched from 8K to 7K, it was observed that the peak intensity increased monotonically with time and did not saturate after more than half an hour. There are, in addition, oscillations identical to those observed in the pure sample. This reveals that the slow dynamics are not caused by poor thermal contacts. The slow dynamics behavior exists even upon change of temperature by an amount as small as 0.05K as shown in Fig. 5(b). The linear relationship in Fig. 5 suggests that the peak intensities are following time logarithmic behavior. In addition to the anomalous behavior of the peak intensity, the peak width also changes continuously. A slow increase of intensity is accompanied by a slow decrease in peak width and *vice versa*. This means that the time dependence originates in slow growth or contraction of the domains after a sudden change in temperature.

To understand the origin of the slow dynamics, we first recall that for SP systems, the phase transition occurs as the neighboring spins pair up and create a local gap in the excitation spectrum, and eventually LRO is achieved when the 3D phase coherence of these local dimerizations is established. In pure CuGeO_3 , these two events happen at the same temperature. For doped samples,

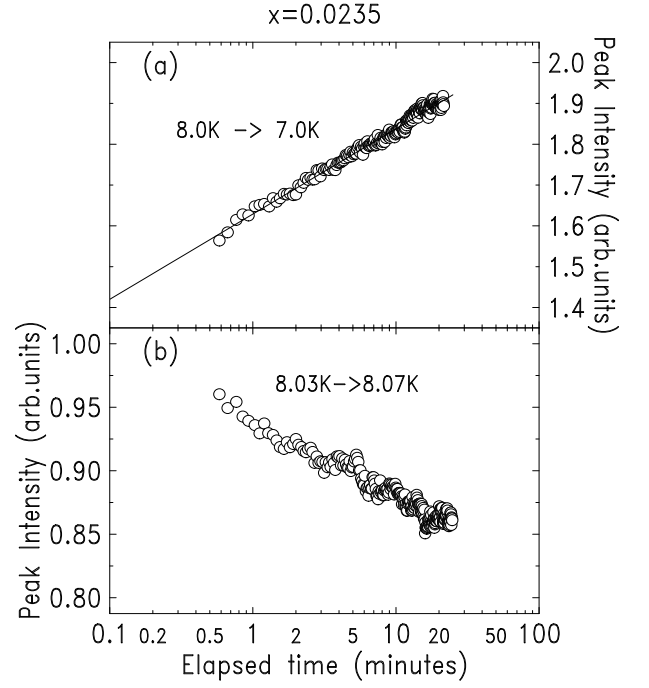


FIG. 5: (a) Semi-logarithmic plot of the peak intensity of the superlattice peak as function of time after a sudden temperature change from 8.0 K to 7.0 K for $x=0.0235$. (b) Similar plot after a temperature change from 8.03 K to 8.07 K.

on the other hand, we observed substantial superlattice intensity even when the system had only SRO, which suggested that SP order had been established locally though the system had difficulty in achieving global phase coherence. Similar behavior has been observed in random field Ising model (RFIM) systems.²⁶ The slow dynamics, then, results from the expansion or contraction of the SRO region as a function of time. However, we do not have quantitative information on the time evolution of the peak width.

C. X-ray scattering – Si doping

As discussed in Sec. I, one of the findings in the studies of doped CuGeO_3 is the close resemblance of the phase diagram for both within-chain and between-chain dopings.^{7,8,10,12,27,28} That is, substitution on the Cu site and substitution on the Ge site have yielded very similar effects on the SP phase, including rapid suppression of the SP transition temperature, occurrence of a low-temperature AF phase, and the concomitant co-existence of the SP and AF phases.

In this section, we describe synchrotron x-ray diffraction experiments on $\text{CuGe}_{1-y}\text{Si}_y\text{O}_3$ samples. As expected, most of our experimental observations are similar to the Zn-doping results presented in the previous section. However, we find that Si-doping is two to three times as effective in destroying the SP phase as compared

to Zn- or Mg- doping, in agreement with earlier workers.⁸

A representative set of longitudinal (parallel to the scattering vector) x-ray scans around the (1.5, 1, 1.5) SP dimerization peak position for the $y=0.0019$, 0.0104, and 0.0171 samples at various temperature is shown in Fig. 6. Similar to the Zn-doping case, the low-temperature SP peak width is resolution limited in the $y=0.0019$ sample, indicating that the SP phase possesses LRO. On the other hand, the SP peaks in the $y=0.0104$ and $y=0.0171$ samples are broadened at all experimentally accessible temperatures, and therefore only SRO is present. To extract the correlation length, the data for all samples were fit to a two-dimensional convolution (longitudinal and transverse directions) of the experimentally measured Gaussian resolution function with the intrinsic cross section taken as Lorentzian squared.

In Fig. 6, the peak intensity and the associated inverse correlation length obtained from the fitting are shown as functions of temperature. For the $y=0.0019$ sample, with less than 0.2% of Si substitution, the SP transition temperature has been reduced by 1 K. However, other than that, the $x=0.0019$ sample behaves analogously to pure CuGeO_3 . The effects of doping can be more obviously seen as we gradually increase the dopant concentrations. For the samples with higher doping levels, smearing of the order parameter onset temperature, which is reminiscent of the behavior in $\text{Cu}_{1-x}\text{Zn}_x\text{GeO}_3$ and $\text{Cu}_{1-x}\text{Mg}_x\text{GeO}_3$, can be identified. In addition, over the whole temperature range studied, the $y=0.0104$ and the $y=0.0171$ samples never achieve LRO and the correlation lengths at low temperatures saturate at the finite values of about 300 Å and 90 Å, respectively. Moreover, for the $y=0.0104$ sample, this saturation of the correlation length at low temperatures is preempted by the low temperature re-entrance of the SP phase, which is characterized by a suppression of the dimerization peak intensity and a concomitant decrease in the correlation length. The re-entrance, as already elaborated in our Mg doping studies,¹⁸ can be understood as arising from local phase separation of the SP and AF micro-regions. For the $y=0.0171$ sample, despite the large error bars due to the low intensity, the reentrance at around 4 K is still observable from the drop in the peak intensity upon cooling from 4.5 K to 4.1 K. This temperature range also includes the Néel temperature of this sample.

D. Phase diagram

In order to construct comprehensive temperature versus impurity concentration phase diagrams from our x-ray scattering and susceptibility measurements, we define two characteristic temperatures, both related to the SP transition but defined by the physics on different length-scales. The higher transition temperature T_m , is defined as the temperature corresponding to the peak temperature of the critical fluctuations as measured from diffuse scattering intensity. We defined the counterpart of T_m

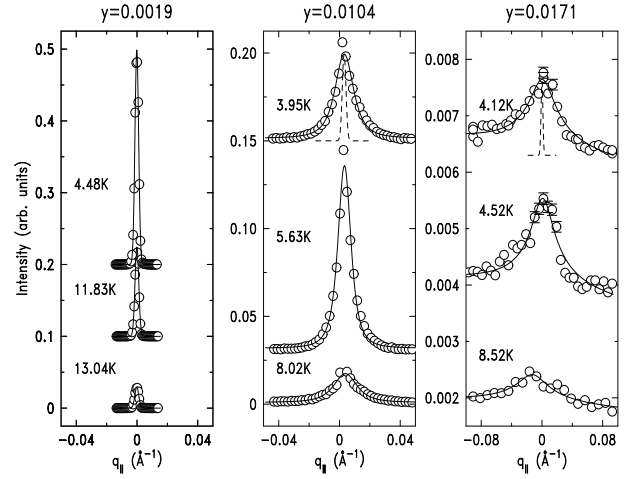


FIG. 6: Representative longitudinal scans at the (1.5, 1, 1.5) SP dimerization peak position. The solid lines are the results of fits to a Lorentzian squared lineshape as described in the text. The instrumental resolution function is shown as dashed lines.

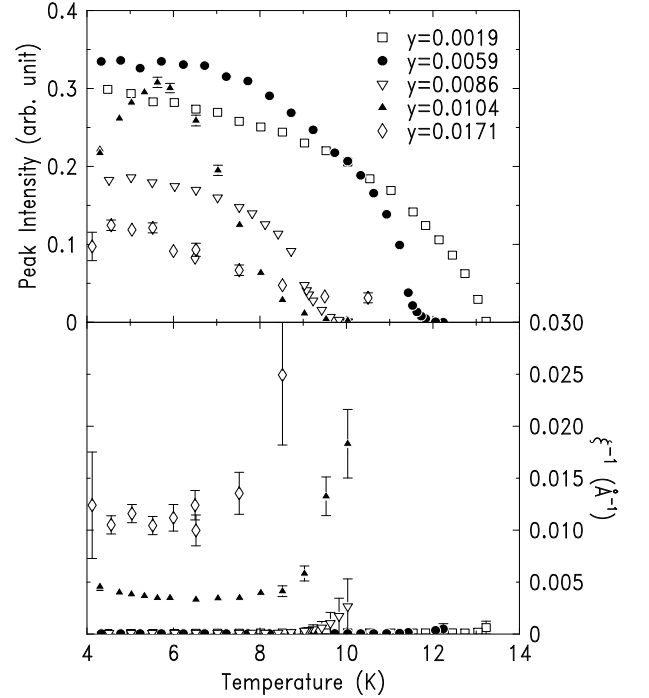


FIG. 7: Peak intensity (top) and inverse correlation length (bottom) of the SP peak as a function of temperature for the $\text{CuGe}_{1-y}\text{Si}_y\text{O}_3$ samples.

in the bulk susceptibility measurements as the temperature at which the derivative of the susceptibility ($d\chi/dT$) reaches a maximum. The lower transition temperature T_s is defined as the temperature at which the lattice dimerization achieved LRO, that is, when the inverse correlation length reaches zero, which in our case means $\xi^{-1} < 0.0002 \text{ Å}^{-1}$.

For the $x=0$ data shown in Fig. 8, there is no am-

biguity in the definition of T_{SP} . The superlattice peak intensity vanishes above $T=14.1$ K while the corresponding correlation length diverges precipitously at the same temperature. In the inset, we show the diffuse scattering intensity at the wing ($\delta q = 2.1 \times 10^{-3} \text{ \AA}^{-1}$) of the dimerization peak. It is clear that the critical fluctuation amplitude reaches a maximum at 14.1 K as well. The susceptibility measurement shown in the bottom panel of Fig. 8 also exhibits a sharp kink anomaly at 14.1 K, at which temperature the derivative shows a sharp peak. From these observations, we find $T_{SP} = T_m = T_s = 14.1$ K for $x=0$. Physically this means that the temperature at which the spin gap appears coincides with the temperature at which long-range coherence of the dimerization is achieved. This perfect agreement by two different techniques, one magnetic and one structural, proves that the SP transition is a well-defined second order phase transition and it also demonstrates the equivalence of the two definitions for the transition temperature. However, as discussed in our previous papers and as is evident from the data presented in this paper, a discrepancy develops between these two definitions as one progresses into the doped regime. It is then difficult to define T_{SP} unambiguously.

In Fig. 9, we show the experimental results for the $x=0.0235$ sample. In the upper panel where x-ray measurements of the dimerization peak are presented, we find smearing of the onset temperature of the order parameter, with substantial intensity starting to appear around 10 K while the critical fluctuation amplitude reaches a maximum around 9.3 K. At the same time, the correlation length does not diverge until the temperature reaches $T_s \approx 7$ K on cooling. In the bottom panel, magnetic susceptibility measurements are shown on the same temperature scale. The kink anomaly corresponding to the SP transition is rounded and the derivative of the susceptibility shows a broad peak around $T_m \approx 9.5$ K. If a linear extrapolation method, which was adopted in Ref. 12, is used, we obtain $T_{SP} \sim 10$ K. These seemingly contradictory results partially explain the difference among the varied phase diagrams reported in the literature.

In Fig. 10, we plot the $T - x$ phase diagram for $\text{Cu}_{1-x}\text{Zn}_x\text{GeO}_3$ using the above definitions from both x-ray and susceptibility results. Our phase diagram is in several ways distinctive: The phase boundaries determined by different definitions of T_{SP} do not match each other except for $x=0$, with the divergence increasing as the doping level increases. The phase boundary determined from T_s is nearly vertical around $x=0.027$. No LRO can be attained above this concentration level, although substantial intensity at the dimerization peak position is still observed. Note that the AF transition in the susceptibility measurement at $x=0.027$ is also broadened. On the other hand, the phase boundary determined from T_m follows an approximately linear variation with the Zn concentration. In particular, for $x=0.034$, while T_s cannot be defined due to the lack of LRO, one can still determine T_m because there still exists substan-

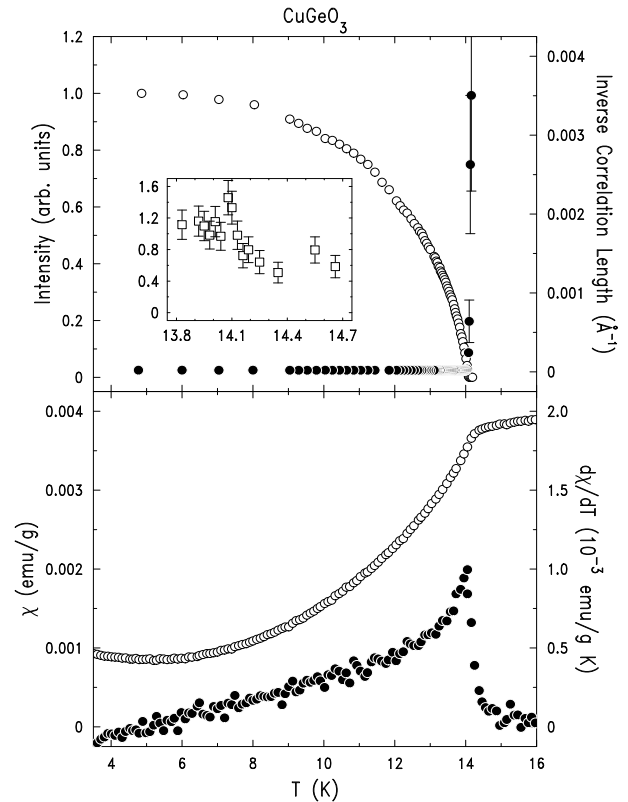


FIG. 8: Top: Temperature dependence of the peak intensity (empty) and the inverse correlation length (filled) of CuGeO_3 . Inset: Temperature dependence of diffuse scattering intensity at $\delta q = 2.1 \times 10^{-3} \text{ \AA}^{-1}$. Bottom: Temperature dependence of the magnetic susceptibility (empty circles) and its temperature derivative (filled circles).

tial intensity at the dimerization peak position in the critical temperature regime.

In Fig. 11, we also present the T - y phase diagram for $\text{CuGe}_{1-y}\text{Si}_y\text{O}_3$.²⁹ The same definitions for T_s and T_m are used. The phase diagram is very similar to those of $\text{Cu}_{1-x}\text{Mg}_x\text{GeO}_3$ and $\text{Cu}_{1-x}\text{Zn}_x\text{GeO}_3$, with a linear suppression of the SP phase upon doping and a critical concentration around $x_c=0.009$, above which no LRO can be observed. The value of $x_c \approx 0.009$ is slightly less than half that of the critical concentration $x_c=0.021$ and $x_c=0.027$ in the Mg- and in Zn-doped cases, respectively. Also, one should note that the slope of the linear line in Fig. 11 is two to three times that in Fig. 10, which suggests that the Si-doping is more than twice as effective in destroying the SP phase as the within-chain Mg and Zn dopants. Previous workers have rationalized this by noting that the Si-dopant affects more than one chain.⁸ In addition, as we shall discuss in the next section, the Si will create a random elastic field on the Cu site which in a pseudo-spin description will act like a random field which is also destructive of the order.

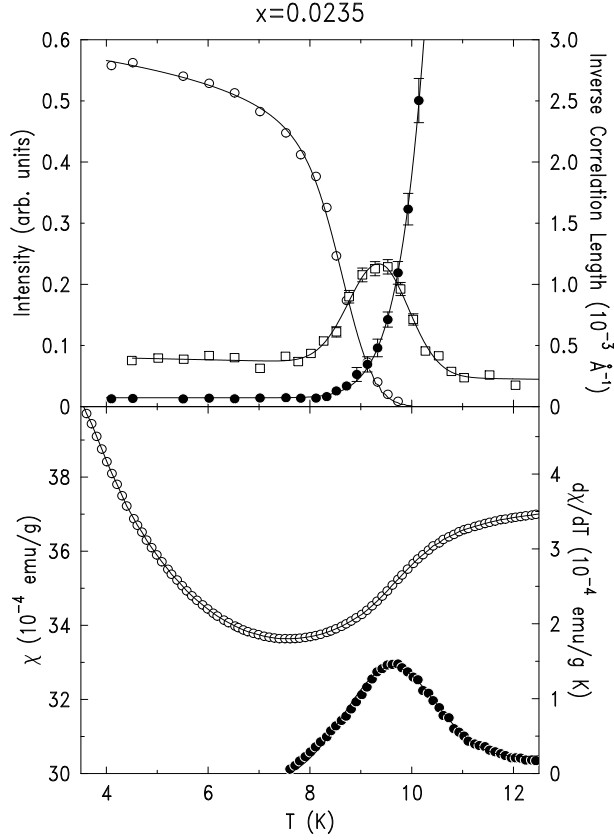


FIG. 9: Top: Temperature dependence of the peak intensity (empty) and the inverse correlation length (filled) of $\text{Cu}_{0.9765}\text{Zn}_{0.0235}\text{GeO}_3$. Also plotted in square symbols is the temperature dependence of the diffuse scattering intensity at $\delta q = 2.2 \times 10^{-2} \text{ \AA}^{-1}$. Bottom: Temperature dependence of magnetic susceptibility (empty) and its temperature derivative (filled).

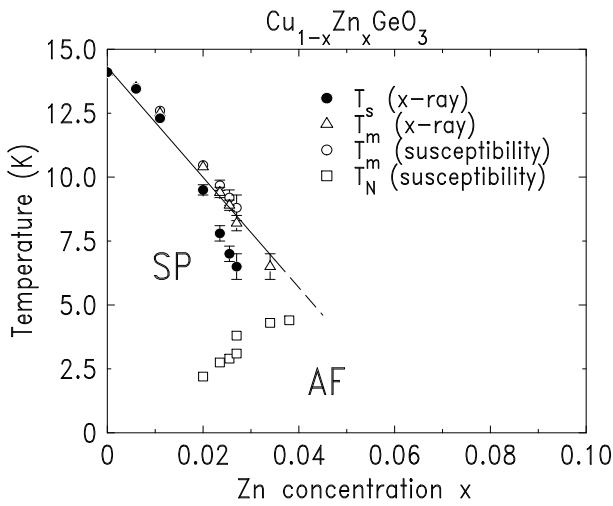


FIG. 10: Experimentally determined $T-x$ phase diagram of $\text{Cu}_{1-x}\text{Zn}_x\text{GeO}_3$.

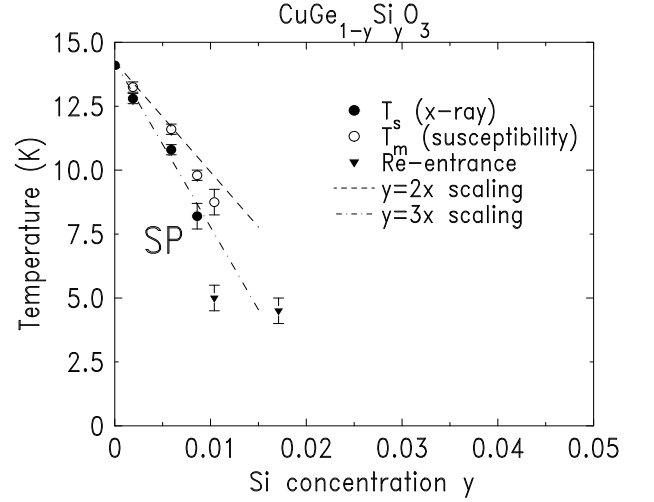


FIG. 11: Experimentally determined $T-y$ phase diagram of $\text{CuGe}_{1-y}\text{Si}_y\text{O}_3$. The solid line shown in Fig. 10 is rescaled to illustrate the $y=2x$ and $y=3x$ scaling.

IV. DISCUSSION

The first conundrum in the diluted CuGeO_3 problem is why the SP phase is destroyed by only $\sim 2\%$ Zn or Mg and even less in the Si case. In comparison, a much higher doping concentration is required to destroy the Haldane gapped state in the $S=1$ spin chain.³⁰ Khomskii *et al.*²⁰ first proposed a soliton model as a starting point for the study of the doped CuGeO_3 problem. The soliton picture is consistent with both numerical simulations^{31,32,33,34} and experiments.^{35,36} However, Khomskii and coworkers note that if diluted CuGeO_3 is treated in a simple percolation picture, then the soliton model naturally yields a critical concentration $x_c \sim 10\%$. Here x_c is determined by the concentration at which the average dopant spacing equals the soliton width. This implies that there must be a separate mechanism that is responsible for the rapid destruction of the SP phase.

In order to discuss this, we follow Harris *et al.*³⁷ and map the dimerized SP system onto an effective 3D Ising model, in which the two dimer configurations possible in a given chain are associated with the up and down states of the Ising pseudo-spins as shown in Fig. 12(a). When a few Cu ions are replaced by Zn ions in an isolated chain, it is energetically favorable for the Ising pseudo-spin to change sign across the Zn dopant. In Fig. 12(b), we show that the dopant effectively creates an antiferromagnetic bond in the ferromagnetic pseudo-Ising model. Note that the dopants can cut the chains into segments with either an even or an odd number of spins in them. The “even” segments favors the dimer configuration in which all the spins are paired, since this configuration has lower energy in comparison with the other one, which has two unpaired spins at the ends of the segments. For the “odd” segment, on the other hand, the two dimer configurations are energetically equivalent. According to numer-

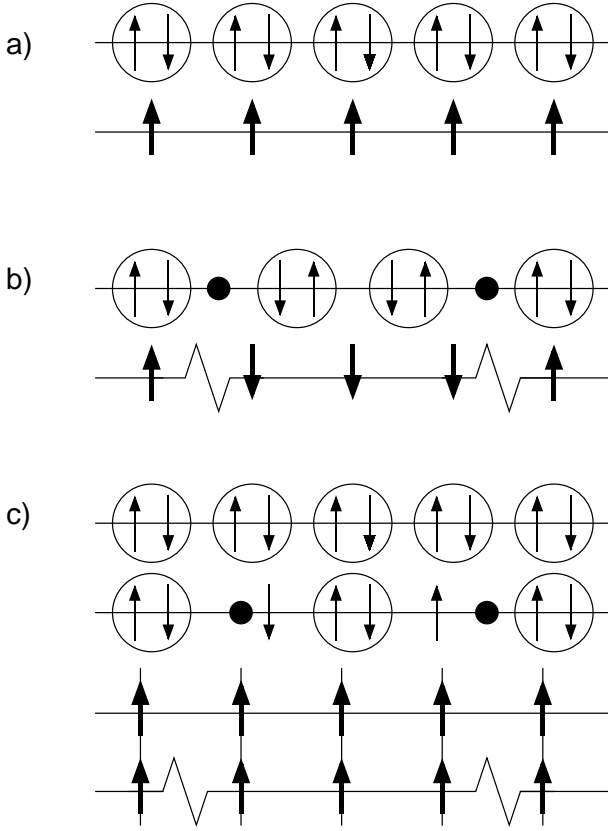


FIG. 12: (a) Pseudo-Ising model mapping for single chain without dopant and (b) with dopant (c) Pseudo-Ising model with interchain interaction

ical simulations,³⁸ however, the soliton in the odd segments prefers to be in the center of the segment, thereby creating two smaller segments with opposite pseudo-Ising spins.

As temperature is lowered, a uniformly ordered phase, as shown in Fig. 12(c) is preferred, since the interchain interaction prefers to keep all the dimers in phase in order to achieve 3D LRO. Therefore, depending on the energetics of the interchain interaction and the soliton creation energy, locally ordered dimers with the “wrong” pseudospin may be flipped at low temperatures. We note a similar mapping by Mostovoy *et al.*,³⁹ in which the equivalent fields were taken to infinity to solve the model.

The essential physics thus involves a competition between the interchain interaction which favors a uniform phase of the dimerization and the local soliton energy which is minimized by a change in phase of the dimerization at the dopant site. It is this competition between intrachain and interchain energies which leads to the fragility of the LRO spin-Peierls state.

Another system of this kind is a magnetic system with both ferro- and antiferromagnetic bonds. For this system, the ordering problem with competing interactions has been well addressed.^{40,41} In particular, Aeppli, Maletta and coworkers proposed a phenomenological cluster spin-glass model^{40,41,42,43,44,45} to explain the evolution of the

ground state from ferromagnetic LRO to spin-glass.

We should emphasize that our observation in doped CuGeO_3 of a Lorentzian squared cross section instead of Lorentzian is significant. By way of contrast, in a simple dilution induced percolation problem,²⁵ even above the percolation threshold, the diffuse scattering should always be Lorentzian, which is characteristic for fluctuations of thermal or geometrical origin only. The occurrence of a Lorentzian squared lineshape implies competing interaction or random field dominated physics.⁴⁶ In the Si-doped case, because of the low symmetry of the Ge site the dopant will generate both competing interchain interactions and random fields. Microscopic calculations are required to determine which are more important quantitatively.

In addition to the unusual SP transition, the AF transitions in doped CuGeO_3 samples also exhibit abnormal characteristics. Neutron scattering experiment on 3.4% (nominal) Zn-doped CuGeO_3 ¹⁹ revealed that the AF order parameter did not saturate even at 1.4 K. In addition, the transition itself was considerably rounded. Fitting the order parameter using a Gaussian distribution of the transition temperature, Hase *et al.* obtained $\beta = 0.22 \pm 0.02$ which did not fit into any extant 3D universality class. In the μSR studies,^{47,48} the Néel ordering process was described as an inhomogeneous process with islands of freezing spins emerging from the paramagnetic phase. Although the transition was mistakenly interpreted in a spin glass picture, it revealed that the Néel transition was not a homogenous process despite the fact that it yields a 3D LRO magnetic state. We believe that the inhomogeneous ordering of the AF transition is due to the coexistence of an inhomogeneous SP phase and the AF phase involving local phase separation.

In order to understand the competition between the SP and AF phases, it is illuminating to compare $\text{Cu}_{1-x}\text{Zn}_x\text{GeO}_3$ with $\text{Cu}_{1-x}\text{Ni}_x\text{GeO}_3$. In the case of Ni-doping case,⁷ due to the non-zero magnetic moment of the Ni ion, the AF ordering takes place at a quite different temperature from that of Zn- or Mg- doping, while the effect on the SP phase boundary seems to be the same. This experimental observation suggests that the SP phase transition and the AF transition should be treated independently, that is, the suppression of the SP ordering can not be simply attributed to the competition from the AF ordering. Although these two phases are intricately correlated as evidenced by the re-entrance of the SP phase upon the onset of the AF phase, the onset of the AF ordering is only indirectly related to the destruction of the SP phase.

As discussed in detail in the section on Si-doping and in Ref. 18, we observed at approximately the same temperature as the onset of the AF ordering, that the SP phase underwent a reentrant transition which was evidenced by the increase in the dimerization peak width upon cooling through Néel temperature. Additionally, the reentrant process was accompanied by slow dynamics and hysteresis. The reentrance and the hysteresis are

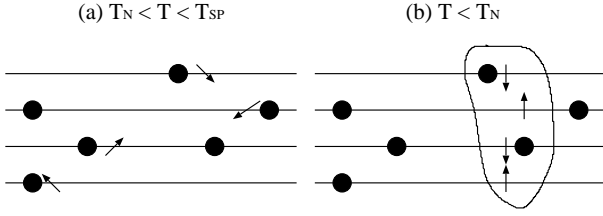


FIG. 13: (a) The free spin configuration above the AF transition and (b) Antiferromagnetically ordered islands below the AF transition.

unusual in the sense that they coincide with the onset of the AF ordering over the doping range studied, which implies that the reentrance is directly related to the AF ordering.

As shown in Fig. 13, we propose a local phase separation scenario to explain this unusual AF transition and the coexistence of the AF and SP phases. As shown in Fig. 12, solitons bear double identities in the system, they involve both structural anti-phase domain walls for the SP phase and the free spins for the underlying magnetic system. For materials with $x < x_c$ or $y < y_c$, the temperature is decreased below the SP transition temperature, the interchain interactions lead to the creation of a LRO SP phase. For even segments, two solitons are created at the end – see Fig. 12(c), while for odd segments, the solitons that were located at the center will move to the end of the segment to bind to the dopants. As a result, a LRO SP order in fact creates many solitons that bind to the dopant sites. These free spins have antiferromagnetic correlations among them, and the dimerized spins will be partially polarized to mediate the magnetic interactions. At the Néel temperature, the spins eventually develop AF order. We believe that the key factor in inducing the reentrance is the non-uniform nature of the AF state. Above the AF transition, the free spins are

disordered. However, as the system is cooled, the antiferromagnetic interaction energy will become relevant. The free spins are actually mobile and can move freely in each segment. However, due to the confining potential of the interchain interactions the solitons become bound to the dopants. The onset of the AF state, however, will compete with this configuration because, the lowest energy state will be achieved by moving all these solitons together, in other words, phase separation into soliton-rich and soliton-poor regions, which will inevitably disrupt the originally established SP order.

The final state is the result of this competition between the SP order and AF order. Since the solitons are bound by the dopants, the phase separation can happen only locally. It is not currently known whether the resulting state involves islands or stripes or some other geometry. Further theoretical work must be done in this direction. Clearly, however, the slow dynamics and re-entrance can naturally be explained in this way.

Acknowledgments

We thank G. Shirane and V. Kiryukhin for valuable discussions, and Doon Gibbs for allowing us to use the 4K close-cycle refrigerator. The work at MIT was supported by the NSF-LTP Program under Grant No. DMR-0071256. Work at the University of Toronto was supported by the Natural Science and Engineering Research Council of Canada. The work at the National Synchrotron Light Source, Brookhaven National Laboratory, was supported by the U.S. Department of Energy, Division of Materials Sciences and Division of Chemical Sciences, under Contract No. DE-AC02-98CH10886. Research at the University of Tokyo was partially supported by Grant-in-Aid for COE Research “SCP Project” from the Ministry of Education, Sports, Science and Technology of Japan.

- ¹ M. Hase, I. Terasaki, and K. Uchinokura, Phys. Rev. Lett. **70**, 3651 (1993).
- ² M. Hase, I. Terasaki, K. Uchinokura, M. Tokunaga, N. Miura, and H. Obara, Phys. Rev. B **48**, 9616 (1993).
- ³ S. Coad, J.-G. Lussier, D. F. McMorrow, and D. McK. Paul, J. Phys.: Condens. Matter **8**, 6251 (1996).
- ⁴ Y. Sasago, N. Koide, K. Uchinokura, M. C. Martin, M. Hase, K. Hirota, and G. Shirane, Phys. Rev. B **54**, R6835 (1996).
- ⁵ M. C. Martin, M. Hase, K. Hirota, G. Shirane, Y. Sasago, N. Koide, and K. Uchinokura, Phys. Rev. B **56**, 3173 (1997).
- ⁶ P. Fronzes, M. Poirier, A. Revcolevschi, and G. Dhalenne, Phys. Rev. B **55**, 8324 (1997).
- ⁷ B. Grenier, J.-P. Renard, P. Veillet, C. Paulsen, R. Calmcsuk, G. Dhalenne, and A. Revcolevschi, Phys. Rev. B **57**, 3444 (1998).
- ⁸ B. Grenier, J.-P. Renard, P. Veillet, C. Paulsen, G.

- Dhalenne, and A. Revcolevschi, Phys. Rev. B **58**, 8202 (1998).
- ⁹ H. Nakao, M. Nishi, Y. Fujii, T. Masuda, I. Tsukada, K. Uchinokura, K. Hirota, and G. Shirane, J. Phys. Soc. Japan **68**, 3662 (1999).
- ¹⁰ T. Masuda, A. Fujioka, Y. Uchiyama, I. Tsukada, and K. Uchinokura, Phys. Rev. Lett. **80**, 4566 (1998).
- ¹¹ Y. J. Wang, V. Kiryukhin, R. J. Birgeneau, T. Masuda, I. Tsukada, and K. Uchinokura, Phys. Rev. Lett. **83**, 1676 (1999).
- ¹² T. Masuda, I. Tsukada, K. Uchinokura, Y. J. Wang, V. Kiryukhin, and R. J. Birgeneau, Phys. Rev. B **61**, 4103 (2000).
- ¹³ M. Hase, I. Terasaki, Y. Sasago, K. Uchinokura, and H. Obara, Phys. Rev. Lett. **71**, 4059 (1993).
- ¹⁴ S. B. Oseroff, S.-W. Cheong, B. Aktas, M. F. Hundley, Z. Fisk, and L. W. Rupp, Jr., Phys. Rev. Lett. **74**, 1450 (1995).

- ¹⁵ J.-G. Lussier, S. M. Coad, D. F. McMorro, and D. McK. Paul, *J. Phys.: Condens. Matter* **7**, L325 (1995).
- ¹⁶ J. P. Schoeffel, J. P. Pouget, G. Dhalenne, and Revolevski, *Phys. Rev. B* **53**, 14971 (1996).
- ¹⁷ K. M. Kojima, Y. Fudamoto, M. Larkin, G. M. Luke, J. Merrin, B. Nachumi, Y. J. Uemura, M. Hase, Y. Sasago, K. Uchinokura, Y. Ajiro, A. Revcolevski, and J.-P. Renard, *Phys. Rev. Lett.* **79**, 503 (1997).
- ¹⁸ V. Kiryukhin, Y. J. Wang, S. C. LaMarra, R. J. Birgeneau, T. Masuda, I. Tsukada, and K. Uchinokura, *Phys. Rev. B* **61**, 9527 (2000).
- ¹⁹ M. Hase, K. Uchinokura, R. J. Birgeneau, K. Hirota, and G. Shirane, *J. Phys. Soc. Japan* **65**, 1392 (1996).
- ²⁰ D. Khomskii, W. Geertsma, and M. Mostovoy, *Czech. J. Phys.* **46**, Suppl. S6 3240 (1996).
- ²¹ H. Fukuyama, T. Tanimoto, and M. Saito, *J. Phys. Soc. Japan* **65**, 1182 (1996).
- ²² Y. J. Wang, Ph.D. thesis, Massachusetts Institute of Technology, 2001.
- ²³ T. Masuda, K. Ina, K. Hadama, I. Tsukada, K. Uchinokura, H. Nakao, M. Nishi, Y. Fujii, K. Hirota, G. Shirane, Y. J. Wang, V. Kiryukhin, and R. J. Birgeneau, *Physica B* **284**, 1637 (1999).
- ²⁴ Y. J. Wang, Y. J. Kim, R. J. Christianson, S. C. LaMarra, F. C. Chou, and R. J. Birgeneau, *Phys. Rev. B* **63**, 052502 (2001).
- ²⁵ R. J. Birgeneau, R. A. Cowley, G. Shirane, and H. Yoshizawa, *J. Stat. Phys.* **34**, 817 (1984).
- ²⁶ Q. Feng, R. J. Birgeneau, and J. P. Hill, *Phys. Rev. B* **51**, 15188 (1995).
- ²⁷ J.-P. Renard, K. L. Dang, P. Veillet, G. Dhalenne, A. Revolevski, and L.-P. Regnault, *Europhys. Lett.* **30**, 475 (1995).
- ²⁸ M. Weiden, R. Hauptmann, W. Richter, C. Geibel, P. Hellmann, M. Koppen, F. Steglich, M. Fischer, P. Lemmens, Guntherodt, A. Krimmel, and G. Nieva, *Phys. Rev. B* **55**, 15067 (1997).
- ²⁹ S. Katano, O. Fujita, J. Akimitsu, M. Nishi, K. Kakurai, and Y. Fujii, *Phys. Rev. B* **57**, 10280 (1998).
- ³⁰ Y. Ajiro, T. Asano, F. Masui, and M. Mekata, *Phys. Rev. B* **51**, 9399 (1995).
- ³¹ M. Ain, J. E. Lorenzo, L. P. Regnault, G. Dhalenne, A. Revcolevski, B. Hennion, and T. Jolicoeur, *Phys. Rev. Lett.* **78**, 1560 (1997).
- ³² M. Arai, M. Fujita, M. Motokawa, J. Akimitsu, and S. M. Bennington, *Phys. Rev. Lett.* **77**, 3649 (1996).
- ³³ A. Dobry and D. Ibaceta, *Phys. Rev. B* **58**, 3124 (1998).
- ³⁴ A. Dobry and D. Ibaceta, *Phys. Rev. B* **59**, 8660 (1999).
- ³⁵ Y. Fagot-Revurat, M. Horvatic, C. Berthier, P. Segransan, G. Dhalenne, and A. Revcolevski, *Phys. Rev. Lett.* **77**, 1861 (1996).
- ³⁶ M. Horvatic, Y. Fagot-Revura, C. Berthier, P. Segransan, and A. Revcolevski, *Phys. Rev. Lett.* **83**, 420 (1999).
- ³⁷ Q. J. Harris, Q. Feng, R. J. Birgeneau, K. Hirota, G. Shirane, M. Hase, and K. Uchinokura, *Phys. Rev. B* **52**, 15420 (1995).
- ³⁸ P. Hansen, D. Augier, J. Riera, and D. Poilblanc, *Phys. Rev. B* **59**, 13557 (1999).
- ³⁹ M. Mostovoy, D. Khomskii, and J. Knoester, *Phys. Rev. B* **58**, 8190 (1998).
- ⁴⁰ G. Aeppli, S. M. Shapiro, H. Maletta, R. J. Birgeneau, and H. S. Chen, *J. Appl. Phys.* **55**, 1628 (1984).
- ⁴¹ G. Aeppli, S. M. Shapiro, R. J. Birgeneau, and H. S. Chen, *Phys. Rev. B* **29**, 2589 (1984).
- ⁴² H. Maletta, *J. Appl. Phys.* **53**, 2185 (1982).
- ⁴³ H. Maletta and W. Felsch, *Z. Phys. B* **37**, 55 (1980).
- ⁴⁴ D. H. Reich, T. F. Rosenbaum, G. Aeppli, and H. J. Guggenheim, *Phys. Rev. B* **34**, 4956 (1986).
- ⁴⁵ D. H. Reich, B. Eelman, J. Yang, T. F. Rosenbaum, G. Aeppli, and D. P. Belanger, *Phys. Rev. B* **42**, 4631 (1990).
- ⁴⁶ R. J. Birgeneau, *J. Mag. Mag. Mat.* **177-181**, 1 (1998).
- ⁴⁷ O. Tchernyshyov, A. S. Blaer, A. Keren, K. Kojima, G. M. Luke, W. D. Wu, Y. J. Uemura, M. Hase, K. Uchinokura, Y. Ajiro, T. Asano, and M. Mekata, *J. Magn. Magn. Mater.* **140-144**, 1687 (1995).
- ⁴⁸ J. L. Garcia-Munoz, M. Suaaidi, and B. Martinez, *Phys. Rev. B* **52**, 4288 (1995).